Petroleum Science 23 (2026) 2885–2901

Contents lists available at ScienceDirect

Petroleum Science

journal homepage: www.keaipublishing.com/en/journals/petroleum-science

Original Paper

# Wax deposition characteristics under oil-water two-phase stratified flow in pipeline

Hui-Shu Liu [a,b], Ji-Miao Duan [b,*], Yong-Xiang Huang [b], Hao-Nan Li [b], Hui-Rong Huang [a,**], Shi-Ming Chen [b], Jun-Zhe Jiang [b]

[a] c tr r v r ty c c T c y 401331
[b] J t t c rt rc v r ty r 401331

A R T I C L E I N F O

rt c t ry:
Received 8 September 2025
Received in revised form
16 November 2025
Accepted 13 January 2026
Available online 20 January 2026

Edited by Teng Zhu and Meng-Jiao Zhou

yw r :
Wax deposition
Oil-water two-phase flow
Stratified flow
Heat and mass transfer

A B S T R A C T

Wax deposition in subsea pipelines transporting waxy crude oil under oil-water stratified flow remains a critical flow assurance challenge. This study systematically investigates wax deposition characteristics using an experimental flow loop that simulates deep-sea conditions. Experiments were conducted with waxy simulated oil and deionized water under varying superficial velocities of both phases. Results show a crescent-shaped deposition layer exclusively on the upper oil-wetted wall, with no deposition on the water-contacted lower wall. Notably, the deposit near the oil-water interface exhibits higher wax content and enriched heavy components compared to the top wall, indicating localized aging behavior. A key finding is that increasing oil or water superficial velocity reduces deposition thickness but enhances wax content and promotes aging. The deposit mass per unit area correlates negatively with oil-phase actual velocity, while wax content and heavy component concentration show strong positive correlations. This work provides novel insights into the circumferential heterogeneity and phase-specific aging of wax deposition in stratified oil-water flow, offering a foundation for improved predictive models.

© 2026 The Authors. Publishing services by Elsevier B.V. on behalf of KeAi Communications Co. Ltd. This is an open access article under the CC BY license (http://creativecommons.org/licenses/by/4.0/).

## 1. Introduction

Under low-temperature conditions in deep water and intense heat exchange, the temperature of crude oil near the pipe wall in subsea waxy oil pipelines decreases below the wax appearance temperature (WAT). Consequently, dissolved wax molecules near the pipe wall crystallize into solid-phase structures, forming three-dimensional networks that deposit via free surface energy onto the pipe wall or existing deposit layers (Wang et al., 2022, 2024). This deposition reduces the pipeline's effective flow area, diminishes transportation capacity, increases energy consumption, and may lead to pipeline blockages—posing significant threats to subsea production safety and flow assurance (Yao et al., 2023; Akbari et al., 2024). As documented in Fig. 1, wax deposition issues have been reported across major global oil-producing regions (Zheng, 2017), establishing this phenomenon as a universal challenge for waxy oil pipelines.

With the proliferation of deepwater and ultra-deepwater drilling in oil and gas production, water is invariably present in waxy oil transmission pipelines (Shafiei et al., 2023; Lekomtsev et al., 2018). Furthermore, during late-stage field extraction, reservoir pressure decline typically necessitates water injection techniques, making oil-water two-phase flow ubiquitous in crude oil transportation. Stratified flow, a prevalent flow pattern in oil-water systems, serves as the fundamental basis for studying complex flow regimes. Therefore, investigation into wax deposition characteristics and predictive modeling for waxy oil-water stratified flow under deepwater low-temperature conditions holds critical importance for both deepwater resource development and pipeline operational safety.

Stratified flow represents a common pattern in oil-water two-phase pipe flow and serves as a fundamental basis for investigating other flow regimes. Nevertheless, experimental research on wax deposition within oil-water stratified flow remains limited due to experimental complexities and the multifaceted nature of

* Corresponding author.
** Corresponding author.
- r : duanjimiao@126.com (J.-M. Duan), hryh@cqust.edu.cn (H.-R. Huang).

Peer review under the responsibility of China University of Petroleum (Beijing).

https://doi.org/10.1016/j.petsci.2026.01.016
1995-8226/© 2026 The Authors. Publishing services by Elsevier B.V. on behalf of KeAi Communications Co. Ltd. This is an open access article under the CC BY license (http://creativecommons.org/licenses/by/4.0/).

influencing factors. Consequently, only a small number of scholars have undertaken experimental studies focused on wax deposition characteristics, and even fewer have developed effective predictive models. Bordalo and Oliveira (2007) employed simulated oil to examine wax deposition in stratified and annular flows. The findings indicate deposition in stratified flow is confined to the upper section of the pipe wall. In contrast, annular flow exhibits deposition across the pipe wall, despite separation of the oil phase from the wall by a water ring. Although this water film inhibits contact between wax particles and the pipe surface, its effectiveness is constrained by the thickness, discontinuous, and intermittent nature of the film. Anosike (2007) separately investigated deposition characteristics using an oil-water two-phase annular channel apparatus, encompassing stratified flow, oil-in-water dispersed flow, water-in-oil dispersed flow, and double-dispersed flow. Observations revealed significant variations in both wax deposition distribution along the inner pipe wall and oil-water heat transfer characteristics across different flow patterns, thereby influencing deposition behavior. Specifically under stratified flow conditions, deposition occurs exclusively on pipe wall regions in direct contact with the oil phase. The deposit layer demonstrates uniform circumferential distribution (except near oil-water interface regions) and exhibits a relatively compliant texture,

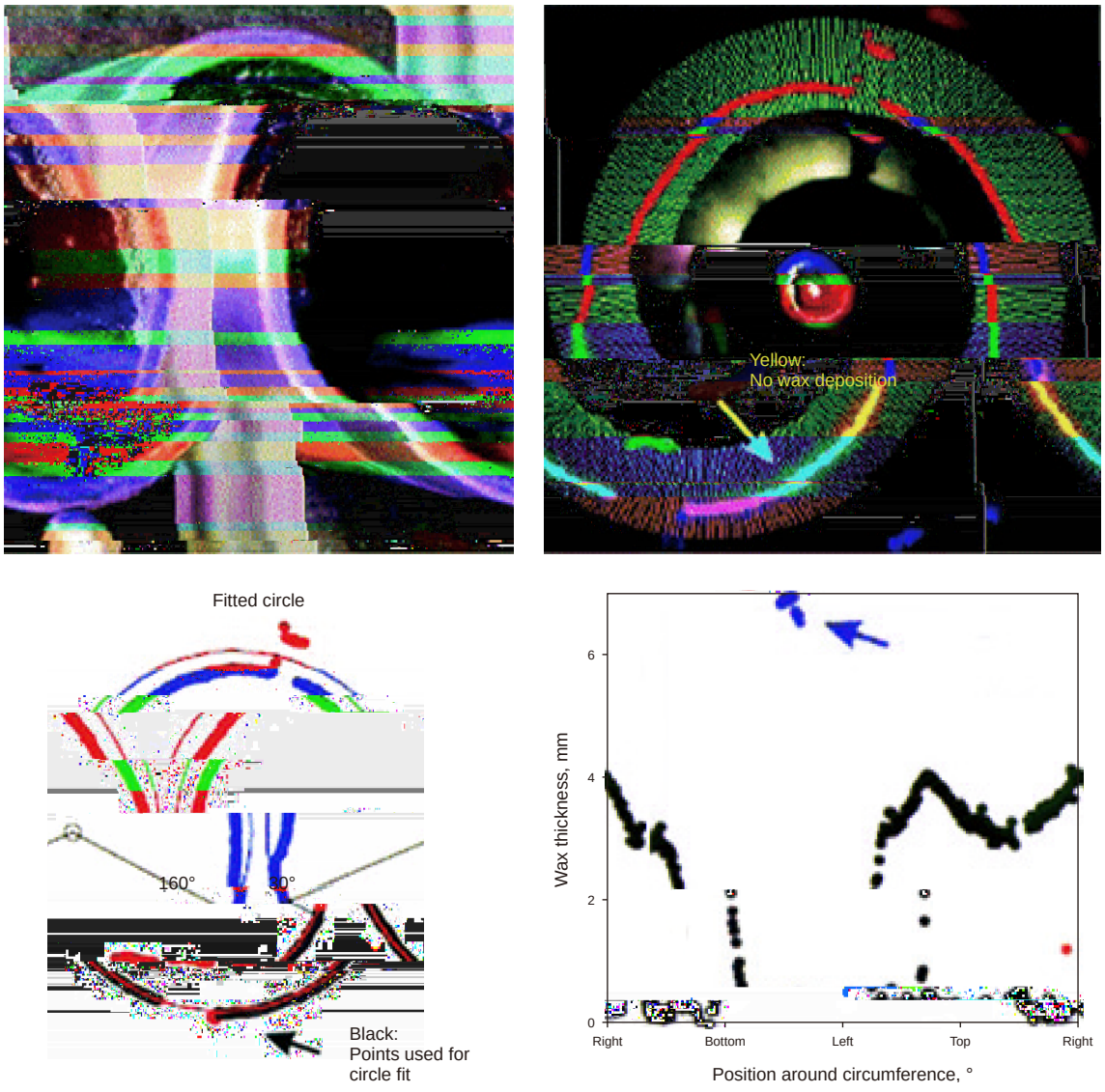


**Fig. 2.** Distribution of wax deposition in the oil-water two-phase stratified flow (Hoffmann et al., 2012).

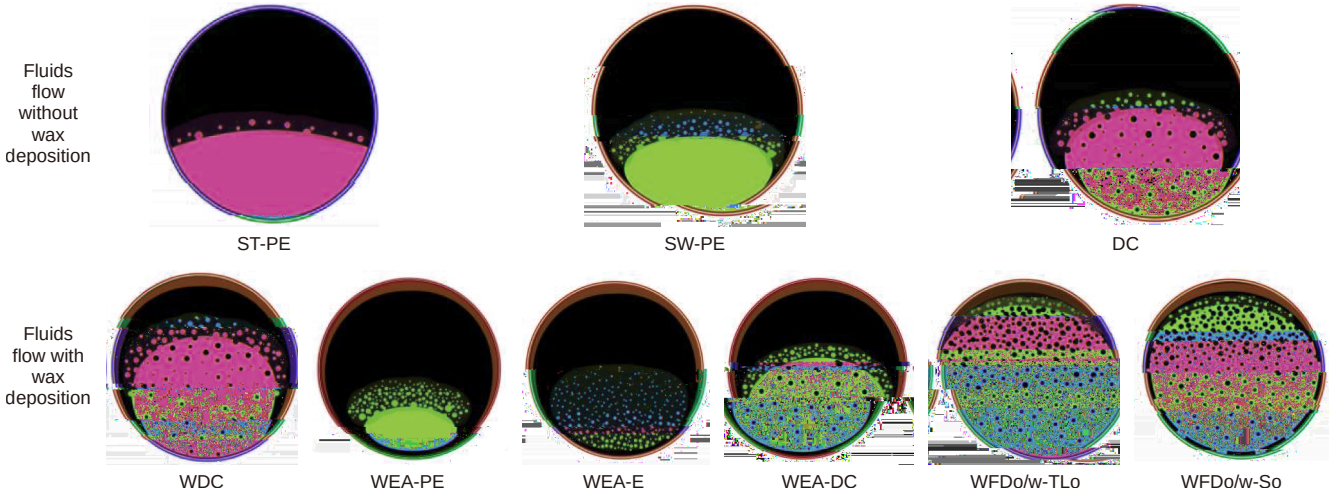


**Fig. 3.** Flow pattern map of waxy crude oil-water two-phase stratified flow in horizontal pipes (Piroozian et al., 2017).

along with the influence of aqueous and oil phase superficial velocities on deposition. Wax content and carbon number distributions of deposits were analyzed by high-temperature gas chromatography (HTGC) at distinct circumferential positions within the pipe cross-section.

## 2. Experimental

Due to the long duration of the oil-water laminar wax deposition loop test, the oil and water phases are subjected to continuous shearing by the pump during the test,

dominant role of wax concentration gradients in deposition dynamics, the complete precipitation state at −20 °C serves as a valid reference for characterizing deposition behavior.

The carbon number distribution of the waxy simulated oil was analyzed by high-temperature gas chromatography (GC 8890, Agilent Technologies, USA), with results shown in Fig. 7. The carbon number distribution analysis reveals the

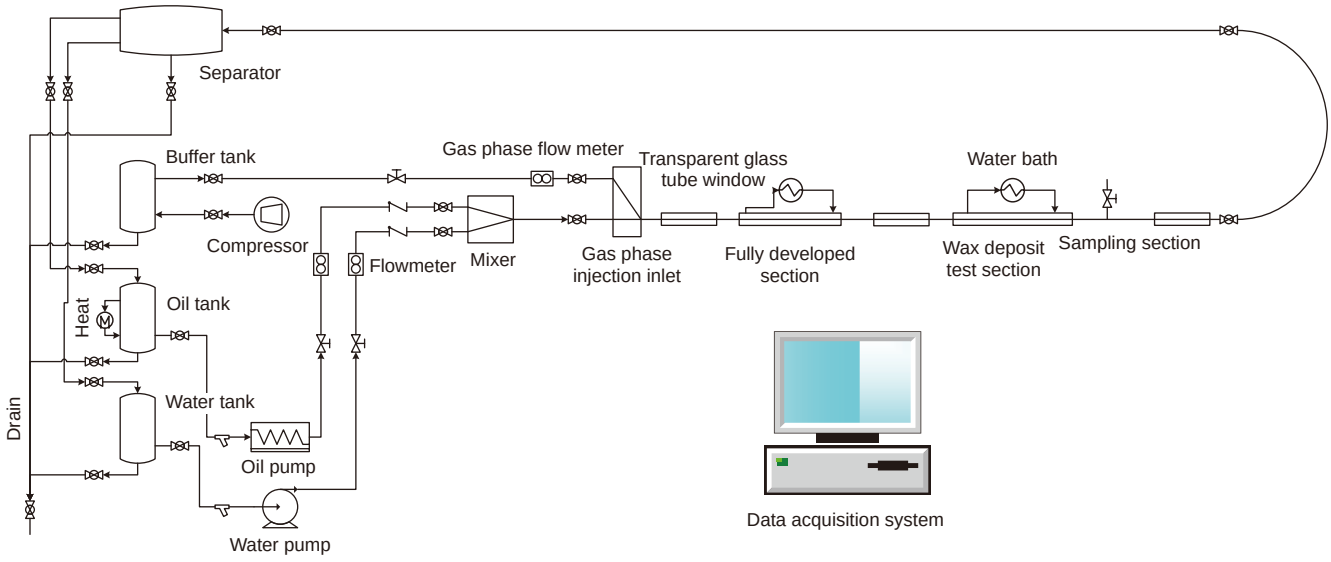


**Fig. 8.** Schematic diagram of wax deposition experiment setup for oil-water two-phase stratified flow.

experiments were conducted at oil phase superficial velocities of 0.10, 0.20, and 0.40 m/s, which encompassed the actual oil-phase flow rate range observed during the two-phase experiments. The comprehensive wax deposition loop experimental program, detailed in Table 2, comprised a total of 36 experimental runs.

### 2.4 c t t t x r t t y

It is crucial to delineate the scope and inherent limitations of this experimental study to clarify the applicability of the presented findings. The conclusions drawn herein are primarily valid under the following specific conditions:

(1) Flow pattern: The investigation was exclusively conducted under stable, laminar oil-water stratified flow. The deposition characteristics may differ significantly in other flow regimes, such as dispersed or slug flow, which are common in field operations.
(2) Fluid properties: The working fluids consisted of a model waxy oil (a binary mixture of paraffin wax and solvent oil) and deionized water. The absence of natural surfactants, asphaltenes, and resins present in live crude oils means that the effects of emulsification and the complex interactions between different crude fractions on wax deposition were not captured.
(3) Operational parameters: The experiments were performed within a defined range of superficial velocities (oil: 0.09–0.30 m/s; water: 0.05–0.34 m/s) and at a fixed temperature differential (oil/water at 30 °C, coolant at 15 °C). Extrapolation of the results beyond these ranges should be done with caution.
(4) Geometric scale: The study utilized a laboratory-scale flow loop with a 25.4 mm internal diameter. Scale effects, which could influence flow hydrodynamics and heat transfer in large-diameter pipelines, were not investigated.

## 3. Results and discussion

### 3.1 t ty x r t r t

The repeatability of experiment is important for ensuring the credibility and reliability of the experimental results. According to the requirements, it is necessary to do a full set of duplication flow loop experiment. Due to the complexity and long duration of the wax deposition experiment, three sets (the second, eighth and tenth) were selected for the repeatability, as shown in Table 2. The three sets of experiments were conducted thrice, for wax deposition durations of 24 h. The average, standard deviation, coefficient of variation of the wax deposition mass and the wax content

**Table 2**
Experimental conditions for wax deposition in an oil-water two-phase stratified flow loop.

| Group | Water phase volumetric flow rate, $m^3/h$ | Oil phase volumetric flow rate, $m^3/h$ | Water phase superficial velocities, m/s | Oil phase superficial velocities, m/s |
|---|---|---|---|---|
| 1 | – | 0.11 | – | 0.10 |
| 2 | – | 0.23 | – | 0.20 |
| 3 | – | 0.45 | – | 0.40 |
| 4 | 0.06 | 0.10 | 0.05 | 0.09 |
| 5 | 0.06 | 0.17 | 0.05 | 0.15 |
| 6 | 0.06 | 0.34 | 0.05 | 0.30 |
| 7 | 0.12 | 0.10 | 0.11 | 0.09 |
| 8 | 0.12 | 0.17 | 0.11 | 0.15 |
| 9 | 0.12 | 0.34 | 0.11 | 0.30 |
| 10 | 0.38 | 0.10 | 0.34 | 0.09 |
| 11 | 0.38 | 0.17 | 0.34 | 0.15 |
| 12 | 0.38 | 0.34 | 0.34 | 0.30 |

**Table 3**
The wax deposition mass for the three repeated experiments.

| Group | First, g | Second, g | Thirth, g | Average, g | Standard deviation, g | Coefficient of variation, % |
|---|---|---|---|---|---|---|
| 2 | 127.65 | 125.03 | 126.35 | 126.34 | 1.31 | 1.04 |
| 8 | 45.65 | 43.36 | 46.53 | 45.18 | 1.64 | 3.62 |
| 10 | 29.69 | 27.63 | 28.45 | 28.59 | 1.04 | 3.63 |

**Table 4**
The wax content in the deposision layer for the three repeated experiments.

| Group | First, wt% | Second, wt% | Thirth, wt% | Average, wt% | Standard deviation, wt% | Coefficient of variation, % |
|---|---|---|---|---|---|---|
| 2 | 21.60 | 20.75 | 21.23 | 21.19 | 0.43 | 2.01 |
| 8 | 22.98 | 21.95 | 23.54 | 22.82 | 0.81 | 3.53 |
| 10 | 23.37 | 21.85 | 22.50 | 22.57 | 0.76 | 3.39 |

in the deposision layer measured from the three repeated experiments are shown in Tables 3 and 4 respectively.

The standard deviations coefficient of variations of the wax deposition mass for the Group 2, 8, 10 three sets of experiments are both relatively small, indicating that the experiment has high repeatability and the experimental setup and methods are highly reliable. The results of the wax content in the deposition layer also indicate this point.

### 3.2 y w x t c r ct r t c -

w

The wax deposition mass and wax deposition mass per unit area under different oil phase superficial velocities are presented in Figs. 9 and 10, respectively. Both parameters exhibit an increase with both deposition time and oil phase superficial velocity. Furthermore, the disparity in wax deposition mass between different oil phase superficial velocities increases over time.

Fig. 11 presents the variation law of wax content in wax deposition with time under different oil phase superficial velocities. When the oil phase superficial velocity remains constant, the wax content in the deposits increases with time. This temporal increase indicates an “aging” phenomenon occurring within the deposition layer, suggesting a corresponding increase in deposit hardness over time. Concurrently, a higher oil phase superficial velocity corresponds to a higher wax content within the deposits. However, the rate of increase in wax content gradually diminishes as the oil phase superficial velocity increases, eventually tending towards stabilization.

Fig. 12 presents the variation in the carbon number distribution within the deposits under different deposition time conditions for an oil phase superficial velocity of 0.40 m/s. As deposition time increases, the proportion of high-carbon-number components

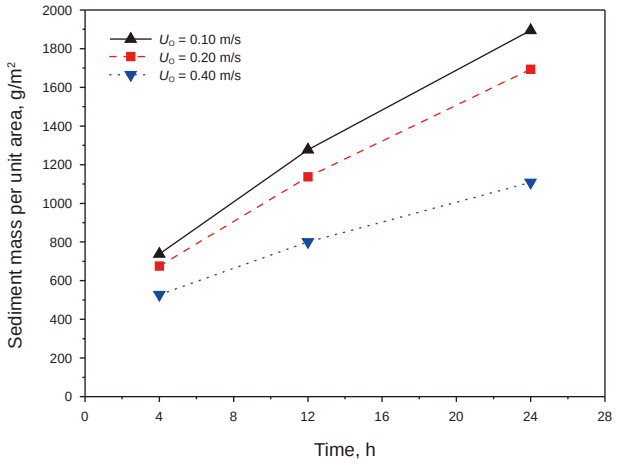


**Fig. 10.** Diagram of the variation law of wax deposition mass per unit area with time under different oil phase superficial velocities.

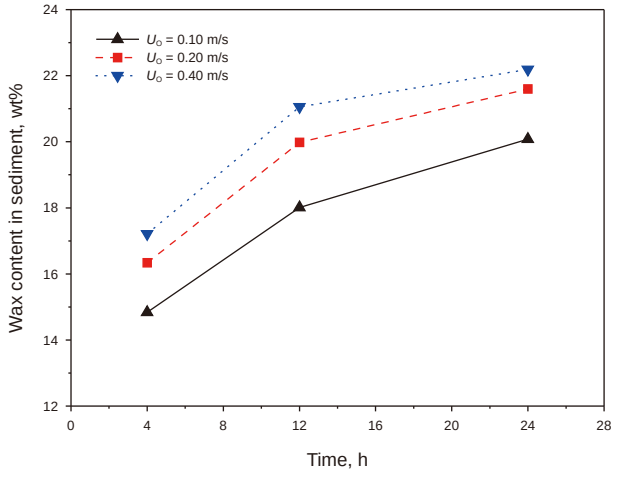


**Fig. 11.** Diagram of the variation law of wax content in deposition with time under different oil phase superficial velocities.

**Fig. 9.** Diagram of the variation law of wax deposition mass with time under different oil phase superficial velocities.

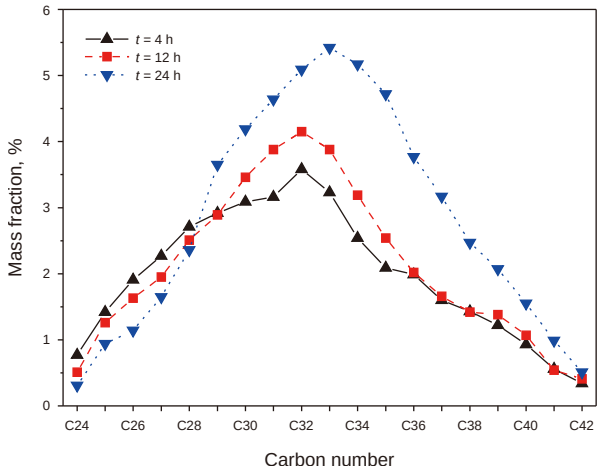


**Fig. 12.** Carbon number distribution in deposition under different deposition time conditions ( $_{o}$ = 0.40 m/s).

(C29–C42) within the deposits increases, while the proportion of low-carbon-number components (C24–C28) decreases, corresponding to an increase in deposit hardness. According to the "aging" mechanism of wax deposition, with prolonged deposition time, wax molecules above C29 originating from the bulk oil flow, the deposit surface, or the shallow deposit layers utilize the liquid oil entrained within the wax deposition layer as a medium. These molecules continue to diffuse into the interior of the deposit layer, subsequently crystallizing and precipitating, thereby increasing the wax content within the deposit layer. Concurrently, as the concentration of wax molecules below C28 within the deposit layer exceeds that in the bulk oil flow, driven by this concentration gradient, molecules below C28 within the deposit layer counter-diffuse towards the oil flow. C28 represents the critical carbon number for this experimental condition.

Fig. 13 illustrates the effects of different oil phase superficial velocities on the carbon number distribution of deposits after 24 h of deposition. The results indicate that within the oil phase superficial velocity range of 0.10–0.40 m/s, increasing the oil flow rate exerts a pronounced effect on deposit composition. The enhanced shear stress associated with higher oil flow rates reduces the amount of oil entrained within the pipe wall deposits,

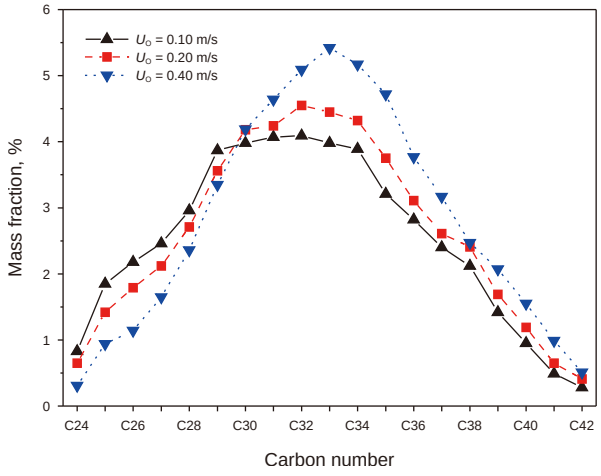


**Fig. 13.** Carbon number distribution in deposition under different oil phase superficial velocities.

thereby aggravating the "aging" effect within the deposit layer. This results in a decrease in low-carbon-number components and a significant increase in the proportion of high-carbon-number components. This phenomenon is primarily attributed to the higher oil phase superficial velocity intensifying convective heat transfer within the pipe. This enhanced heat transfer increases the temperature gradient at the deposit-oil flow interface, promoting the deposition of higher-molecular-weight fractions (high-carbon-number components).

The observed increase in wax content and the enrichment of high-carbon-number components with time and flow rate point to the occurrence of deposit aging. This phenomenon is attributed to a synergistic interplay between molecular diffusion and shear stress. The aging process is fundamentally driven by molecular diffusion, wherein dissolved wax molecules (particularly higher alkanes) from the bulk flow continue to diffuse into the deposit layer and precipitate, while entrapped liquid oil (richer in lighter components) diffuses out, driven by concentration gradients (Li et al., 2020; Huang et al., 2011). Shear stress, intensified at higher flow rates, acts as a critical accelerator of this process. It compacts the deposit matrix, reducing its porosity and the amount of occluded oil. This compaction shortens the internal diffusion path lengths and promotes a more effective expulsion of light components, thereby leading to a denser, harder deposit with an accelerated enrichment of heavy waxes. Therefore, while diffusion dictates the compositional shift, shear stress controls the kinetics and the final physical state of the aged deposit.

### 3.3 y w x t c r ct r t c tw w

#### 3.3.1 x t c r ct r t c cr ct

The circumferential distribution pattern of wax deposition on the pipe wall cross-section in oil-water two-phase stratified flow is closely related to the flow pattern, analogous to wax deposition behavior observed in oil-gas two-phase stratified flow (Goncalves and Matar, 2022; Chi et al., 2019; Duan et al., 2017). Different flow patterns yield distinct deposit distribution patterns and circumferential variations in deposit wax content (Anosike, 2007; Hoffmann et al., 2012; Piroozian et al., 2017). Therefore, to elucidate the wax deposition characteristics of oil-water stratified flow, investigation of local deposition characteristics across the pipe cross-section is essential.

#### 3.3.1.1 tr t t y r t cr - ct

Fig. 14(a) shows the morphology of the deposit layer on the inner pipe wall cross-section after disassembly, following 24 h of deposition under superficial oil-phase velocity $_{so}$ = 0.09 m/s and superficial water-phase velocity $_{sw}$ = 0.11 m/s. Under the oil-water laminar flow conditions, the deposit morphology exhibits a crescent shape. Wax deposition occurs only on the upper pipe wall section in contact with the oil phase. No wax deposition occurred on the lower pipe wall in contact with water. The main reason might be that the aqueous phase acted as a barrier, resulting in the pipe wall lacking direct contact with the oil phase. The thickness of the deposit layer on the entire cross-section of the pipe was measured at 20° intervals around the pipe using a square and a calibrated needle. The needle with scale has an accuracy of 0.05 mm. Considering that the needle may undergo slight deformation when inserted into soft deposits, it is estimated that the measurement error is within ±0.02 mm. The variation of deposit layer thickness with the angle ($\alpha$) from the pipe center is shown in Fig. 14(b). The deposit layer near the top of the pipe wall ($\alpha \approx 0°$) has a relatively uniform thickness of approximately 4.71 mm.

Progressing circumferentially along the pipe wall towards the oil-water interface, the deposit layer thickness decreases.

To further analyze wax deposition characteristics across the pipe cross-section, the deposition layer was divided into three parts: top (T), left side (L) and right side (R) of the contact part of the phase interface according to the distribution morphology of the deposition layer on the pipe wall. The wax contents of deposits from the top, left, and right pipe wall regions, measured via high-temperature gas chromatography, were 18.21%, 23.19%, and 22.96%, respectively. The wax contents of the left and right deposit layers were essentially identical. Relative to the top deposit layer, regions near the oil-water phase interface exhibited thinner deposits with higher wax content. This finding aligns with direct morphological observations: the deposit on the top inner pipe wall was softer, while deposits on the left and right sides were harder and firmer.

Fig. 15 exhibits the carbon number distributions of deposits from the top, left, and right pipe wall regions. The alkane compositions of the left and right deposits were similar, while the top deposit contained fewer high-carbon-number components. This result is consistent with the measured wax content data. Unlike single-phase flow, where the deposit-oil flow interface temperature and thermal boundary layer are uniformly distributed circumferentially, the oil-water two-phase stratified flow exhibits circumferential variation in this distribution. Different n-alkane components possess distinct physical properties (e.g., solubility, molecular diffusivity), leading to differing mass transfer and precipitation characteristics at the deposit surface (Li et al., 2020).

*3.3.1.2 ct t t* Fig. 16 shows the morphology distribution of the deposit layer on the inner pipe wall cross-section after 4, 12, and 24 h of deposition under superficial oil-phase velocity $_{so} = 0.09$ m/s and superficial water-phase velocity $_{sw} = 0.11$ m/s. The deposit thickness at the pipe crown increases with deposition time. Conversely, the vertical distance from the pipe crown to the bottom of the deposit layer remains essentially constant throughout the deposition period. This indicates that under the given flow conditions, the deposit layer exerts negligible influence on the oil-phase-wetted perimeter.

The wax content of the deposits at the top and side of the pipe wall and all deposits of the test section of the pipe with deposition times of 4, 12 and 24 h were measured by high temperature gas chromatog DTGpjTp3DADAD3DADADTnp 8tuA3AmDADAD3DADBTp3DADA

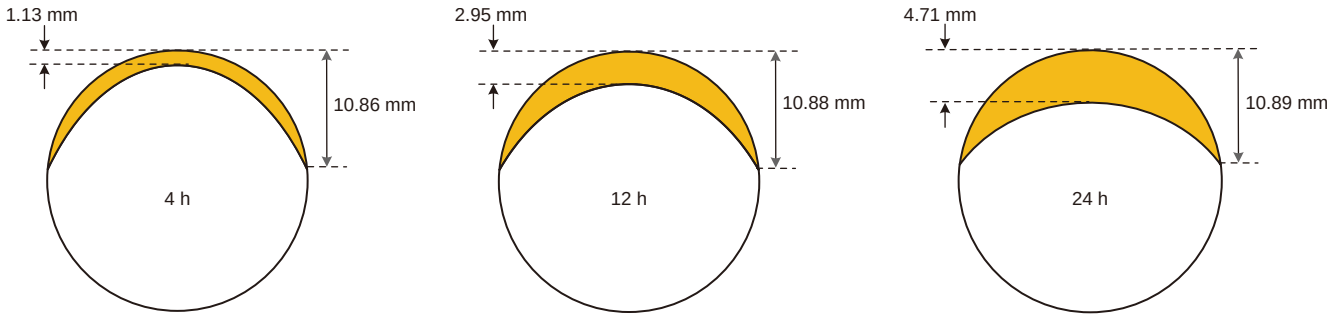


**Fig. 16.** Morphological distribution of the deposition layer on the inner wall cross-section of the pipeline.

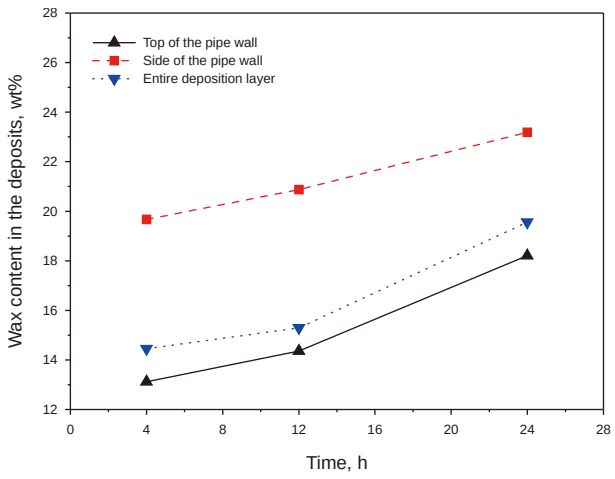


**Fig. 17.** Diagram of the variation law of wax content in deposition with time on the top and side surfaces of the pipe wall.

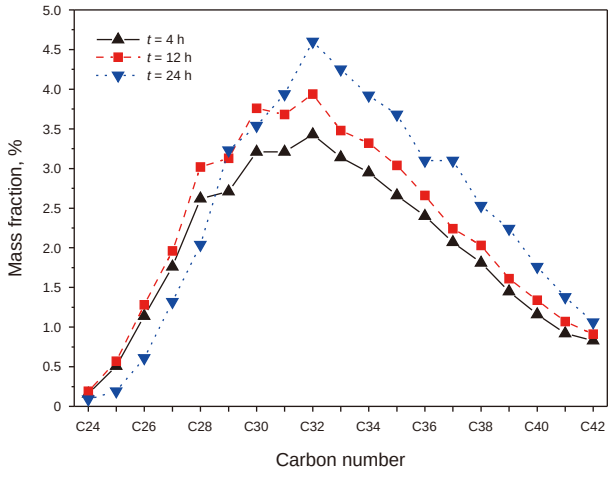


**Fig. 19.** Carbon number distribution of deposits on the pipe wall side.

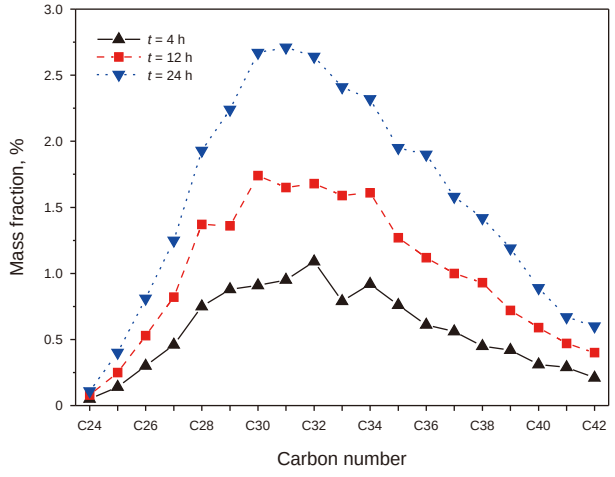


**Fig. 18.** Carbon number distribution of deposits on the pipe wall top.

and 19, it can be concluded that, compared with the side of the pipe wall, the top of the pipe wall has fewer components in the same deposition time, and the content of high carbon number alkanes is low at the initial moment of deposition, and the "aging" tendency of the deposition layer is more obvious.

### 3.3.2 ct w t r c v c t w x t

Wax deposition experiments were conducted at an oil phase superficial velocity so = 0.15 m/s and wate phase superficial velocities sw = 0.05, 0.11, and 0.34 m/s, respectively, to investigate the influence of different water phase superficial velocities on wax deposition in stratified oil-water two-phase flow. Fig. 20 presents the variation of deposition mass with deposition time at different water phase superficial velocities for a fixed oil phase superficial velocity of so = 0.15 m/s. The results show that the deposition mass increases with time. In addition, at the same deposition time, the deposition mass decreases with increasing water phase superficial velocity.

In oil-water two-phase stratified flow, the oil phase occupies only the upper section of the pipe. Consequently, wax deposition occurs exclusively on the pipe wall wetted by the oil phase in this upper region and is absent on the pipe wall wetted by the water phase in the lower section. The area of the pipe wall wetted by the oil phase varies with flow conditions, leading to differences in the surface area covered by wax deposition. Therefore, characterizing the wax deposition rate using the mass of deposits per unit deposition area (i.e., the deposit mass divided by the wetted area where deposition occurs) under stratified oil-water flow conditions provides a more scientifically sound and reasonable approach.

Fig. 21 illustrates the perimeter of the pipe wall wetted by the oil phase in the pipe cross-section under different water phase apparent velocities. The results indicate that this wetted perimeter decreases with increasing water phase superficial velocity but increases with increasing oil phase superficial velocity. This implies that a larger surface area is available for wax deposition as the oil phase superficial velocity increases or the water phase superficial velocity decreases. This observed trend agrees with

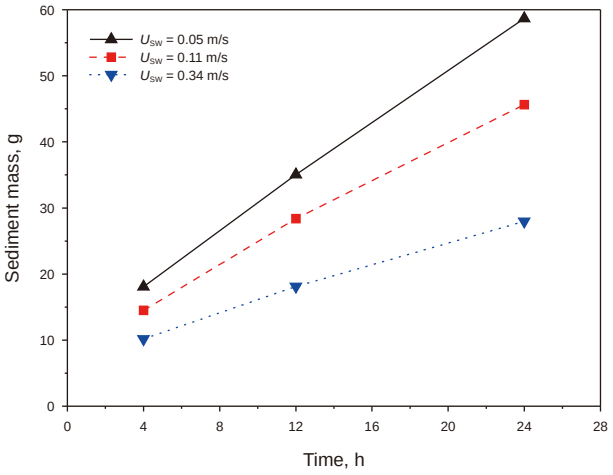


**Fig. 20.** Diagram of the variation law of wax deposition mass with time under different wate phase superficial velocities.

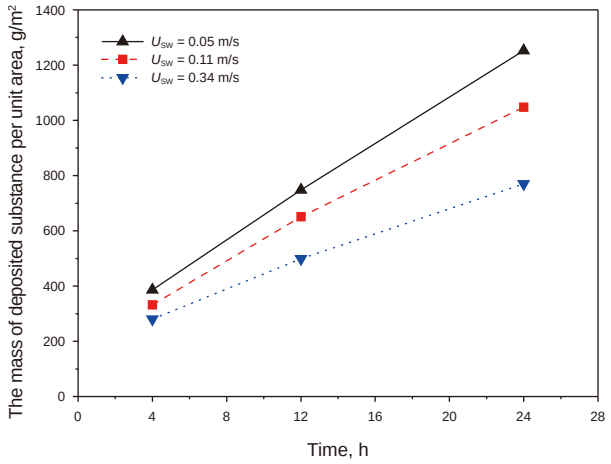


**Fig. 22.** Diagram of the variation law of wax deposition mass per unit area with time under different wate phase superficial velocities.

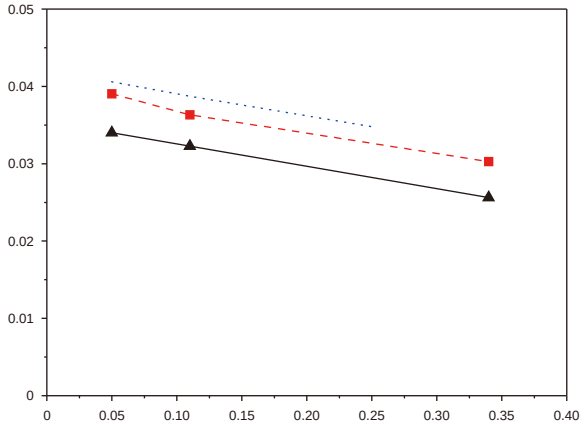

**Fig. 21.** The perimeter of the pipe wall wetted by the oil phase in the pipe cross-section under different water phase apparent velocities.

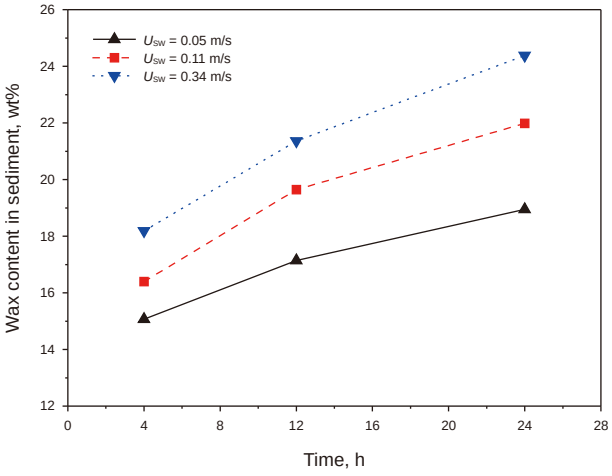


**Fig. 23.** Diagram of the variation law of wax content in deposition with time under different wate phase superficial velocities.

calculations from the stratified oil-water two-phase flow model developed by Ullmann et al. (2004). Additionally, Santos et al. (2019) and Edomwonyi-Out and Angeli (2015) also experimentally observed that the perimeter wetted by the oil phase decreases with increasing water phase superficial velocity.

Fig. 22 shows the variation of wax deposition mass per unit area with time under different water phase superficial velocities for a fixed oil phase superficial velocity $_{so} = 0.15$ m/s. As observed for the total deposition mass trend, the deposition mass per unit area decreases with increasing water phase superficial velocity This trend is consistent with the experimental results of Hoffmann et al. (2012) for wax deposition under oil-water two-phase stratified flow. Specifically, Hoffmann et al. (2012) measured deposition mass per unit area values of 1643.8 and 705.2 g/m$^2$ in oil-water two-phase stratified flow loop experiments at oil phase superficial velocities of 0.33 m/s combined with water phase superficial velocities of 0.33 and 0.98 m/s, respectively.

Fig. 23 presents the wax content in deposition under different water phase superficial velocities. The results demonstrate that the wax content in the deposition layer gradually increases with increasing water phase superficial velocity. At a constant oil phase superficial velocity, the oil volume fraction in the pipe cross-section decreases as the water phase superficial velocity increases. This increase in the actual oil-phase flow velocity leads to higher shear stress on the deposition layer surface. Consequently, this promotes the formation of more interlocked solid-phase wax crystals, resulting in a deposition layer with higher shear yield stress, higher hardness, and higher wax content (Yao et al., 2023; Santos et al., 2021).

The diffusive mass flow of wax molecules from the main body of the oil flow to the surface of the deposition layer, $_{wax}$, is a key parameter for wax deposition prediction modeling (Soedarmo et al., 2017) and corresponds to the slope of the deposition mass per unit area versus time plot. Fig. 24 shows the variation of the wax molecular diffusive mass flux $_{wax}$ with time at different water phase superficial velocities for a fixed oil phase superficial velocity $_{so} = 0.15$ m/s. The results indicate that $_{wax}$ decreases with deposition time. This decrease occurs because the deposition layer on the pipe inner wall increases thermal resistance, reducing heat transfer from the oil flow to the environment. Additionally, $_{wax}$ decreases with increasing water phase superficial velocity, which aligns with the experimental trend observed in Fig. 22.

The influence of different water phase superficial velocities on wax deposition across the pipe cross-section under oil-water two-phase stratified flow was also examined. Fig. 25 presents the

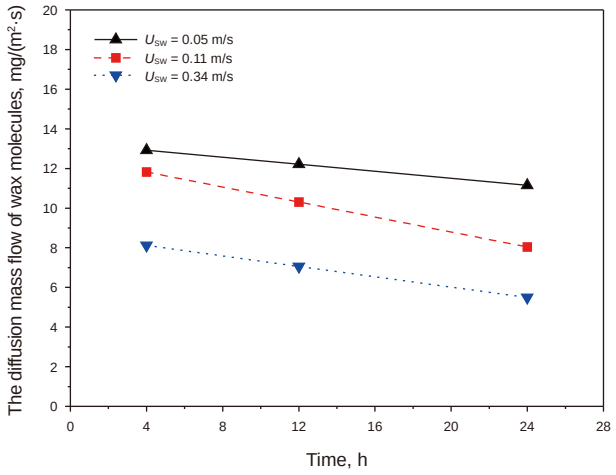


**Fig. 24.** Diagram of the variation law of diffusive mass flux of wax molecules with time under different wate phase superficial velocities.

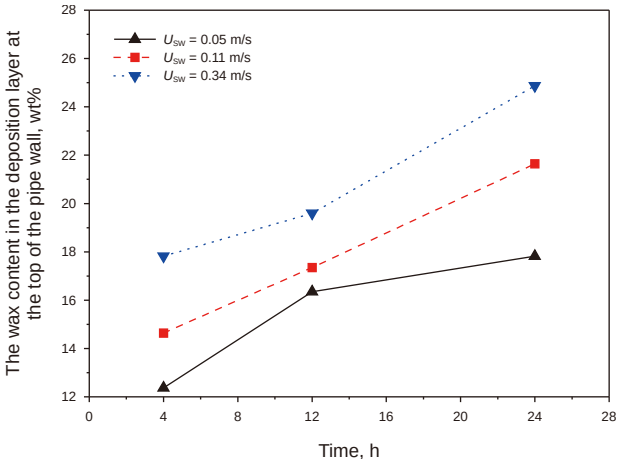


**Fig. 26.** Diagram of the variation law of wax content in the deposition layer on the top of the pipe wall with time under different wate phase superficial velocities.

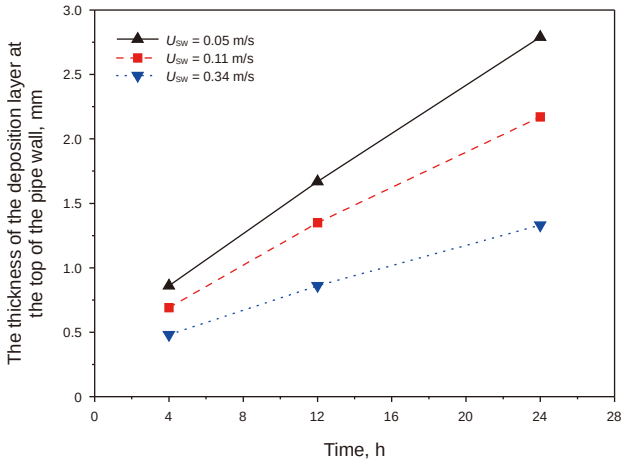


**Fig. 25.** Diagram of the variation law of the thickness of the deposition layer on the top of the pipe wall with time under different wate phase superficial velocities.

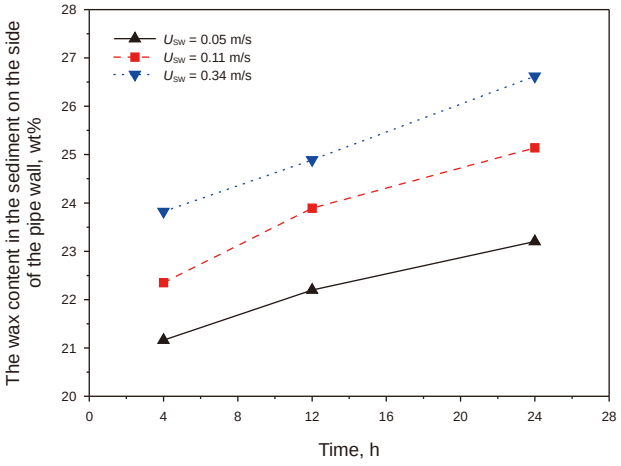


**Fig. 27.** Diagram of the variation law of wax content in the deposition layer on the side of the pipe wall with time under different wate phase superficial velocities.

variation of deposition layer thickness at the top of the pipe wall with deposition time for an oil phase superficial velocity $_{so}$ = 0.15 m/s and different water phase superficial velocities. It can be observed that the deposition layer thickness increases with time. Furthermore, at the same deposition time, the deposition layer thickness decreases with increasing water phase superficial velocity.

Figs. 26 and 27 present the variation of wax content in the deposits on the top and side of the pipe wall, respectively, with deposition time for different water phase superficial velocities at a fixed oil phase superficial velocity. It can be observed that the deposits at both the top and side locations exhibit the “aging” phenomenon: the wax content increases with deposition time, consistent with the trend shown in Fig. 17. Furthermore, at the same deposition time, the wax content on both the top and side of the pipe wall increases with increasing water phase superficial velocity.

This increase in wax content is primarily attributed to the following sequence of effects. As the water phase superficial velocity increases, the oil volume fraction in the pipe cross-section decreases, reducing the flow area available for the oil phase. Consequently, the actual oil phase superficial velocity increases. This higher flow velocity generates greater shear stress on the deposition layer surface. The increased shear stress promotes the formation of a deposition layer with higher shear yield stress and higher wax content.

Figs. 28 and 29 present the carbon number distributions of the deposits on the top and side of the pipe wall, respectively. The results show that the content of high-carbon-number components in the deposits increases with increasing water phase superficial velocity. This trend further confirms that an increase in water phase superficial velocity promotes the “aging” phenomenon observed in the deposition layer at both the top and side locations. Furthermore, comparison of the carbon number distributions between the top and side deposits reveals that the water phase superficial velocity has a more pronounced effect on the carbon number distribution at the side of the pipe wall.

### 3.3.3 ct r c v ct w x t

Wax deposition experiments were conducted at $_{sw}$ = 0.34 m/s and $_{so}$ = 0.09, 0.15, and 0.30 m/s, respectively, to investigate the influence of different oil phase superficial velocities on wax deposition under oil-water two-phase stratified flow. Figs. 30 and 31 present the variation of deposition mass and deposition mass per unit area with deposition time for different $_{so}$ at a fixed

$_{sw}$ = 0.34 m/s. The results show that both deposition mass and deposition mass per unit area increase with time. However, at the same deposition time, deposition mass and deposition mass per unit area decrease with increasing oil phase superficial velocity.

Studies by the research group led by Prof. Fogler at the University of Michigan, USA (Huang et al., 2011a, 2011b, 2011c; Lu et al., 2012; Zheng et al., 2013), demonstrate that the growth rate of the wax deposition layer is primarily governed by the diffusive mass flow of wax molecules, $_{wax}$, from the bulk oil flow to the deposition layer surface. Furthermore, these studies indicate that wax mass transfer normalized per unit area of the deposit layer is the direct cause of pipeline wax deposition formation. Therefore, the variation of deposit mass per unit area with time and oil phase superficial velocity is mainly attributable to the variation in $_{wax}$. Fig. 32 shows the variation of $_{wax}$ with time for different $_{so}$ at a fixed $_{sw}$ = 0.34 m/s. The results indicate that $_{wax}$ decreases with increasing $_{so}$. This trend is consistent with the experimental observations presented in Fig. 31.

Fig. 33 shows the oil-phase wetted perimeter in the pipe cross-section at different $_{so}$. The results indicate that the oil-phase wetted perimeter ( $_{o}$) increases with increasing $_{so}$. This implies greater surface area availability for wax deposition at higher $_{so}$.

Under oil-water two-phase stratified flow conditions, a higher $_{so}$ provides more surface area for wax deposition. At the same deposition time, the total deposition mass decreases with increasing $_{so}$. This phenomenon occurs because the reduction in deposition mass per unit area with increasing $_{so}$ exceeds the magnitude of the increase in available deposition surface area. Fig. 34 presents the wax content of deposits at different $_{so}$. The results demonstrate that the wax content in deposition layer gradually increases with increasing $_{so}$. The higher $_{so}$ generates increased shear stress on the deposition layer surface. Consequently, the resulting deposit exhibits higher shear yield stress, greater hardness, and elevated wax content.

Similarly, the influence of oil-phase apparent flow rate on wax deposition on the pipe cross-section under stratified flow was studied. Fig. 35 presents the variation of deposition layer thickness on the top of the pipe wall with deposition time for different $_{so}$ at a fixed $_{sw}$ = 0.34 m/s. The results reveal that the

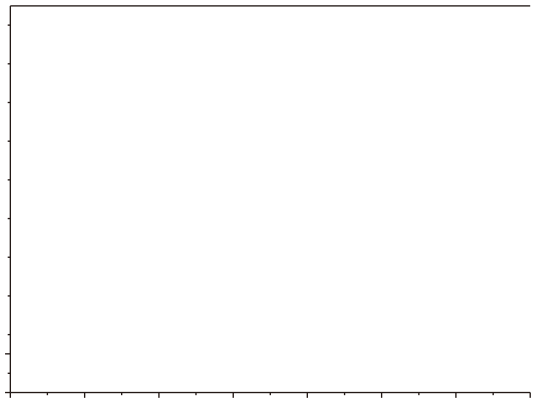

**Fig. 32.** Diagram of the variation law of the mass flux of wax molecules due to diffusion with time under different oil phase superficial velocities.

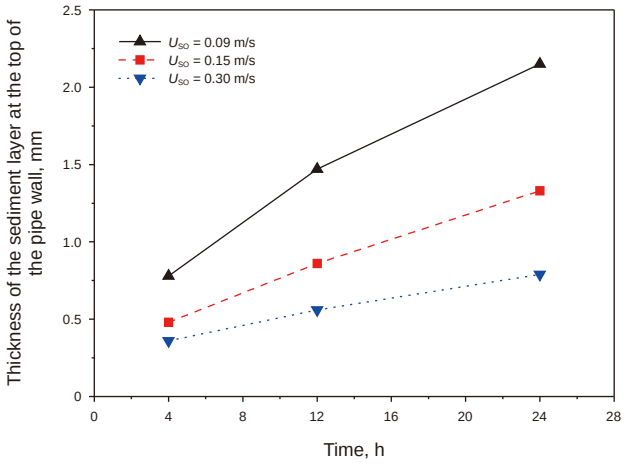


**Fig. 35.** Diagram of the variation law of the thickness of the deposition layer on the top of the pipe wall and time under different oil phase superficial velocities.

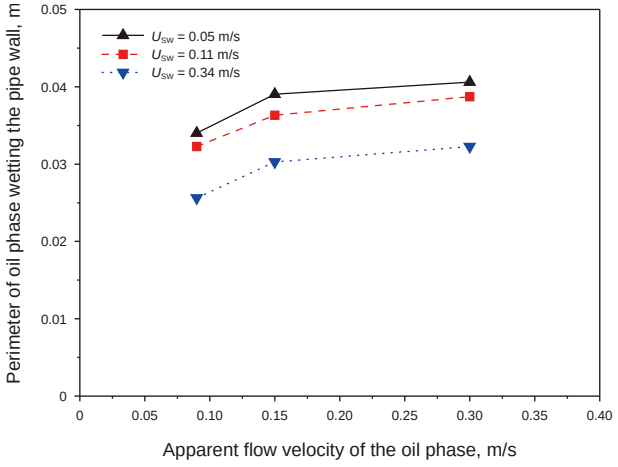


**Fig. 33.** The perimeter of the pipe wall wetted by the oil phase in the pipe cross-section under different oil phase apparent velocities.

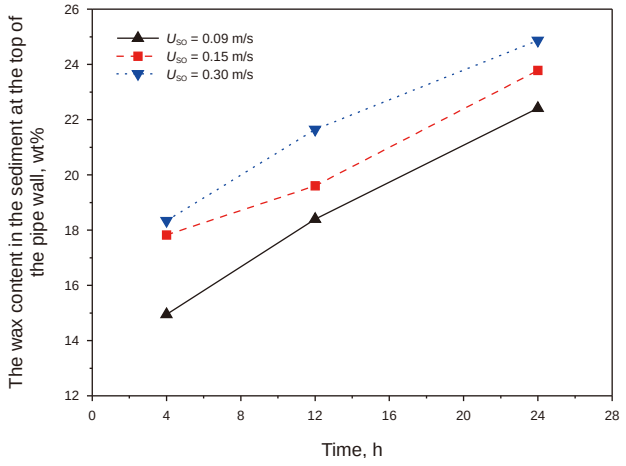


**Fig. 36.** Diagram of the variation law of wax content in the deposition layer on the top of the pipe wall with time under different oil phase superficial velocities.

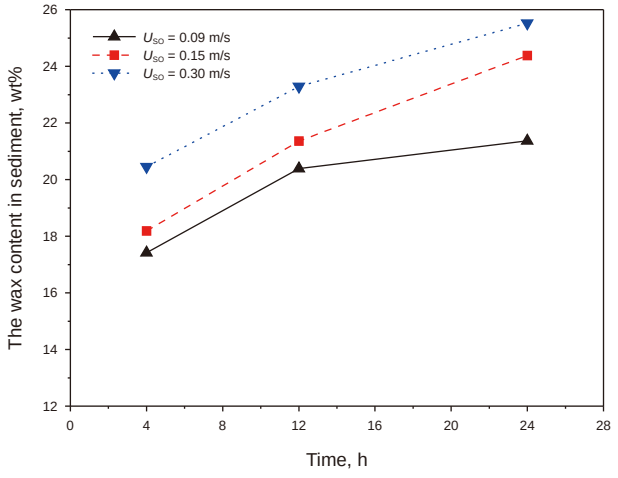


**Fig. 34.** Diagram of the variation law of wax content in deposition with time under different oil phase superficial velocities.

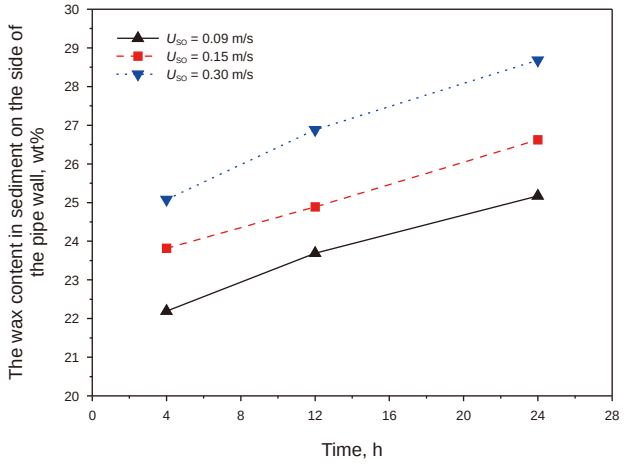


**Fig. 37.** Diagram of the variation law of wax content in the deposition layer on the side of the pipe wall with time under different oil phase superficial velocities.

It can be seen that the deposits at the top and side of the pipe cross-section wall show the phenomenon of “aging” of the deposited layer. Under the same deposition time, with the increase of the apparent oil phase flow rate, the wax content of the deposits at the top and side of the pipe cross-section also shows an increasing trend. This is mainly due to the higher shear stress on the surface of the deposited layer by the increase of the actual flow rate of the oil phase, which leads to higher shear yield stress in the deposited layer and higher content of wax crystals in the deposits.

Figs. 38 and 39 show the carbon number distribution patterns of the deposition on the top and side of the pipe wall in the pipe cross-section at different apparent oil-phase flow rates, respectively. The content of high carbon number components in the deposition increases with the increase of oil-phase apparent flow rate, which also indicates that the oil-phase apparent flow rate promotes the “aging” of the deposition layer at the top and side of the pipe wall. This is not in agreement with the pattern of liquid-phase apparent flow rate influence on the wax deposition characteristics on the pipe cross-section in oil-gas two-phase stratified flow. In oil-gas two-phase stratified flow, the increase of liquid-phase apparent flow rate has less effect on the carbon number distribution of the bottom and side deposits of the pipe. This is mainly due to the compressibility of the gas phase, and an increase in the apparent liquid-phase flow rate causes only a small increase in the actual liquid-phase flow rate. However, an increase in the apparent flow rate of the oil phase during oil-water two-phase stratified flow causes a larger increase in the actual flow rate of the oil phase, which leads to a larger change in the shear stress of the oil flow on the surface of the deposition layer.

*3 4 r t v y w x t*
*w tw*

In single-phase wax deposition, the oil phase actual velocity is closely related to the shear effect and ater nt

area decreases as the oil phase actual velocity increases. However, the reduction in deposition mass observed in two-phase flow is more pronounced than that in single-phase flow.

Fig. 42 shows the difference in wax content of deposits after 24 h between single-phase flow and oil-water two-phase stratified flow conditions. The results indicate that under single-phase flow, the wax content increases with increasing actual oil-phase flow velocity, exhibiting a relatively gentle growth trend. Similarly, in oil-water two-phase stratified flow, the wax content demonstrates a more pronounced increase with increasing the oil phase actual velocity.

The comparison of wax deposition in oil-water two-phase stratified flow versus single-phase flow indicates that the wax deposition model for two-phase flow, which is based solely on local heat transfer parameters and the physical properties of fluid mixing from the single-phase flow model, exhibits significant discrepancies. Therefore, it is essential to accurately characterize the influences of flow dynamics, as well as heat and mass transfer properties, on wax deposition during oil-water two-phase stratified flow in order to reliably predict wax accumulation in pipelines operating under two-phase conditions.

hx

Anosike, C.F., 2007. Effect of Flow Patterns on oil-water Flow Paraffin Deposition in Horizontal Pipes. University of Tulsa.
Bordalo, S.N., Oliveira, R.D., 2007. Experimental Study of oil/water Flow with Paraffin Precipitation in Submarine Pipelines. In: SPE Annual Technical Conference and Exhibition, SPE-110810-MS. https://doi.org/10.2118/110810-MS.
Chi, Y., Sarica, C., Daraboina, N., 2019. Experimental investigation of two-phase gas-oil stratified flow wax deposition in pipeline. Fuel 247, 113–125. https://doi.org/10.1016/j.fuel.2019.03.032.
Duan, J., Liu, H., Jiang, J., Liu, H., Jiang, J., Xue, S., Wu, J., Gong, J., 2017. Numerical prediction of wax deposition in oil–gas stratified pipe flow. Int. J. Heat Mass Tran. 105, 279–289. https://doi.org/10.1016/j.ijheatmasstransfer.2016.09.082.
Edomwonyi-Out, L.C., Angeli, P., 2015. Pressure drop and holdup predictions in horizontal oil–water flows for curved and wavy interfaces. Chem. Eng. Res. Des. 93, 55–65. https://doi.org/10.1016/j.cherd.2014.06.009.
Goncalves, G.F.N., Matar, O.K., 2022. Mechanistic modelling of two-phase slug flows with deposition. Chem. Eng. Sci. 259 (0), 117796. https://doi.org/10.1016/j.ces.2022.117796.
Hoffmann, R., Amundsen, L., Huang, Z., et al., 2012. Wax deposition in stratified oil/water flow. Energy Fuels 26 (6), 3416–3423. https://doi.org/10.1021/ef2018989.
Huang, Z., Lee, H.S., Senra, M., 2011a. A fundamental model of wax deposition in subsea oil pipelines. AIChE J. 57 (11), 2955–2964. https://doi.org/10.1002/aic.12517.
Huang, Z., Lu, Y., Hoffmann, R., et al., 2011b. The effect of operating temperatures on wax deposition. Energy Fuels 25 (11), 5180–5188. https://doi.org/10.1021/ef201048w.
Huang, Z., Senra, M., Kapoor, R., et al., 2011c. Wax deposition modeling of oil/water stratified channel flow. AIChE J. 57 (4), 841–851. https://doi.org/10.1002/aic.12307.
Lekomtsev, A.V., Ilyushin, P.Y., Martyushev, D.A., 2018. Experience of implementing an intensifying device on the developed Mobile well production treatment unit. Chem. Petrol. Eng. 54 (3–4), 213–219. https://doi.org/10.1007/s10556-018-0465-4.
Li, R., Huang, Q., Zhang, D., Zhu, X., Shan, J., Wang, J., 2020. An aging theory-based mathematic model for estimating the wax content of wax deposits using the Fick's second law. AIChE J. 66 (4), 16892. https://doi.org/10.1002/aic.16892.
Lu, Y., Huang, Z., Hoffmann, R., et al., 2012. Counterintuitive effects of the oil flow rate on wax deposition. Energy Fuels 26 (7), 4091–4097. https://doi.org/10.1021/ef3002789.
Piroozian, A., Hemmati, M., Ismail, I., Manan, M.A., Rashidi, M.M., Mohsin, R., 2017. An experimental study of flow patterns pertinent to waxy crude oil-water two-phase flows. Chem. Eng. Sci. 164 (1), 313–332. https://doi.org/10.1016/j.ces.2017.02.026.
Quan, Q., Wang, W., Wang, P., Duan, J., Yang, J., Yao, H., Gong, J., 2015. Wax deposition from emulsion-water in stratified flow. Petrol. Sci. Technol. 33 (6), 749–755. https://doi.org/10.1080/10916466.2015.1007381.
Santos, D.S., Faia, P.M., Garcia, F.A.P., Rasteiro, M.G., 2019. Oil/water stratified flow in a horizontal pipe: simulated and experimental studies using EIT. J. Petrol. Sci. Eng. 174 (0), 1179–1193. https://doi.org/10.1016/j.petrol.2018.12.002.
Santos, G., Daraboina, N., Sarica, C., 2021. Dynamic microscopic study of wax deposition: particulate deposition. Energy Fuels 35 (15), 12065–12074. https://doi.org/10.1021/acs.energyfuels.1c01684.
Shafiei, M., Kazemzadeh, Y., Martyushev, D.A., Dai, Z., Riazi, M., 2023. Effect of chemicals on the phase and viscosity behavior of water in oil emulsions. Sci. Rep. 13 (1), 2045–2322. https://doi.org/10.1038/s41598-023-31379-0.
Soedarmo, A.A., Daraboina, N., Sarica, C., 2017. Validation of wax deposition models with recent laboratory scale flow loop experimental data. J. Petrol. Sci. Eng. 149, 351–366. https://doi.org/10.1016/j.petrol.2016.10.017.
Ullmann, A., Goldstein, A., Zamir, M., Brauner, N., 2004. Closure relations for the shear stresses in two-fluid models for laminar stratified flow. Int. J. Multiphas. Flow 30 (7–8), 877–900. https://doi.org/10.1016/j.ijmultiphaseflow.2004.03.008.
Wang, J., Hao, Y., Zhu, B., Han, T., Li, Z., Zhang, J., 2022. Crystalline behavior of paraffin wax. J. Phys. Chem. B 126 (4), 985–995. https://doi.org/10.1021/acs.jpcb.1c10000.
Wang, C., Ma, Q., Lv, X., Zhang, J., Liu, Y., Zhou, S., 2024. Experimental study on wax deposition of highly paraffinic oil in intermittent gas-oil flow in pipelines. Pet. Sci. 21 (3), 2080–2088. https://doi.org/10.1016/j.petsci.2024.01.003.
Yao, B., Zhu, H., Yan, B., Li, C., Yang, F., Sun, G., Zeng, H., 2023. Pre-heating temperature induced flowability and wax deposition characteristics of crude oil adding wax inhibitors. Pet. Sci. 4, 2468–2478. https://doi.org/10.1016/j.petsci.2023.02.030.
Zheng, S., 2017. Wax Deposition from Single-phase Oil Flows and water-oil Two-phase Flows in Oil Transportation Pipelines. University of Michigan. https://hdl.handle.net/2027.42/137101.
Zheng, S., Zhang, F., Huang, Z., et al., 2013. Effects of operating conditions on wax deposit carbon number distribution: theory and experiment. Energy Fuels 27 (12), 7379–7388. https://doi.org/10.1021/ef402051n.